



1 Global patterns of directed soil moisture influence on air 2 temperature

3 Xiaohang Guo¹, Jichong Han^{1*}, Huaiyong Shao¹, Xinyan Zhu¹, Xiaofei Sun¹, Long Ling¹, Zimeng

4 Chen¹, Gang Liu¹

5 ¹ College of Geography and Planning, Chengdu University of Technology, Chengdu 610059, China

6 *Corresponding author: Jichong Han (hanjichong@cdut.edu.cn)

7 Abstract

8 Soil moisture regulation of near-surface air temperature is essential for improving global climate
9 prediction skill. Yet conventional statistical methods are often insufficient to establish causality, and
10 the dominant pathways of this coupling remain poorly understood at the global scale. Here we
11 combine multiple datasets with the information flow method to quantify the effects of soil moisture
12 on temperature. We find that significant soil moisture–temperature causality exists over about 37%
13 of the global land area. This causality is dominated by the evaporative and sensible heat pathways,
14 affecting 33.5% and 18.5% of land area, respectively, while both pathways co-occur over an
15 additional 7.6% of land area. In addition, these strong causal relationships are mainly driven by soil
16 moisture variability, while most CMIP6 models tend to overestimate the likelihood of such coupling.
17 Our study identifies the main characteristics of land–atmosphere interactions from a causal
18 perspective and provides an important scientific basis for improving land-surface processes in future
19 climate models.

20

21 Keywords: Soil moisture; air temperature; information flow; causal analysis; climate models



22 1. Introduction

23 Soil moisture regulation of near-surface air temperature is crucial for improving our
24 understanding of global climate dynamics(Miralles et al., 2012; Santanello et al., 2018; Seneviratne
25 et al., 2010). Understanding land – atmosphere coupling is essential for predicting extreme heat and
26 drought events(Chiang et al., 2021; Miralles et al., 2019; Zhou et al., 2024). As global warming
27 intensifies, surface energy partitioning becomes increasingly complex. Therefore, accurately
28 quantifying the soil moisture – temperature relationship is vital to understand terrestrial water cycle
29 dynamics and constrain future climate models.

30 Recent studies have extensively examined the interactions between soil moisture and air
31 temperature(Gevaert et al., 2018; Maraun et al., 2025; Zhou et al., 2024). While these studies have
32 highlighted strong soil moisture – temperature coupling, most of these studies rely on Pearson
33 correlation or empirical statistical models(Hirschi et al., 2011; Miralles et al., 2012; Schwingshackl
34 et al., 2017). However, conventional statistical approaches are often insufficient to establish
35 causality, because correlation does not necessarily imply a physical driving mechanism(Hagan et
36 al., 2019; Liang, 2016). The information flow technique has been demonstrated to effectively
37 analyse soil moisture – precipitation causality(Ebert-Uphoff and Deng, 2012; Runge et al., 2019;
38 Sugihara et al., 2012; Sun et al., 2025). However, how soil moisture causally regulates air
39 temperature—and through which dominant pathways—remains unclear at the global scale. In
40 particular, the respective contributions of evapotranspiration and surface sensible heat flux to
41 temperature regulation remain poorly separated(Fu et al., 2024; Hsu and Dirmeyer, 2023).

42 Climate models are the primary tools for assessing future land – atmosphere feedbacks. Many



43 studies using CMIP6 simulations have evaluated changes in surface energy fluxes and associated
44 land - climate interactions (Day et al., 2025; Hsu and Dirmeyer, 2023; Zhou et al., 2025).
45 Nevertheless, the extent to which CMIP6 models can accurately reproduce this feedback remains
46 uncertain (Giardina et al., 2025; Green et al., 2024; Hsu and Dirmeyer, 2023). Meanwhile, previous
47 studies on the drivers of coupling strength have mainly focused on the climatological mean state of
48 soil moisture. By contrast, emerging evidence suggests that soil moisture variability may be an
49 important control on strong land-atmosphere coupling (Hsu and Dirmeyer, 2023; Nouri and Homae,
50 2021; Sun et al., 2025). However, it remains unknown whether this variability-driven relationship
51 extends to soil moisture - temperature causality, and to what extent current CMIP6 models can
52 accurately capture such complex interactions.

53 To address these issues, we employ the Liang - Kleeman information flow method to quantify
54 the causal pathways linking global soil moisture to near-surface air temperature. By decomposing
55 this coupling into evapotranspiration and sensible heat pathways, we investigate the physical
56 processes mediating these land - atmosphere interactions. Furthermore, we analyze how soil
57 moisture variability modulates the strength of these causal links. By comparing these observational
58 findings with historical simulations from 10 CMIP6 models, we assess their capability and potential
59 biases in reproducing this variability-driven coupling.

60



61 2. Materials and methods

62 2.1 Datasets

63 We use the ERA5-Land reanalysis produced by the European Centre for Medium-Range
64 Weather Forecasts for the period 1984 – 2014. ERA5-Land is adopted as the primary reference
65 dataset because it provides globally consistent, physically coherent land-surface and near-surface
66 atmospheric variables required for the causal analysis. We extract monthly data for surface soil
67 moisture (SSM) across four depth layers: Layer 1 (0–7 cm), Layer 2 (7–28 cm), Layer 3 (28–100
68 cm), and Layer 4 (100–289 cm), together with 2-m air temperature (T), evapotranspiration (ET),
69 and surface sensible heat flux (SH). These variables are used for the subsequent causal analysis and
70 physical pathway decomposition.

71 We further analyse historical simulations from 10 CMIP6 models for 1984–2014 (Table S1),
72 selected according to data availability, variable completeness, and model structural diversity. The
73 main variables considered are surface soil moisture and near-surface air temperature. To ensure
74 spatial consistency, all model outputs are bilinearly interpolated onto a uniform 1° grid. This
75 processing facilitates multi-model ensemble averaging and direct comparison with the reanalysis-
76 based results. These simulations are used to evaluate the ability of advanced climate models to
77 reproduce land – atmosphere feedback processes.

78 We also use surface soil moisture (0 – 10 cm) from the Global Land Evaporation Amsterdam
79 Model (GLEAM, version 4.2a) dataset for the period 1984 – 2014 (Miralles et al., 2025). As an
80 observationally constrained product, GLEAM provides a reliable reference for land – atmosphere



81 coupling. It therefore serves as an independent benchmark to verify the robustness of our results.

82 Although the near-surface soil moisture definitions differ slightly among ERA5-Land, GLEAM,

83 and CMIP6, all of them represent surface or near-surface soil water conditions.

84 We deseasonalized all monthly variables before the causal analysis. For each grid cell, the

85 climatological mean of each calendar month was calculated over the full study period, and the

86 corresponding monthly mean was then subtracted from the original series to obtain anomalies.

87 2.2 Causal analysis framework

88 2.2.1 Liang–Kleeman information flow analysis

89 We use the Liang – Kleeman information flow framework to quantify the causal relationship

90 between soil moisture and temperature. Unlike conventional correlation analysis, this method

91 measures the net contribution of the variation in one variable to the evolution of another(Liang,

92 2016; Sun et al., 2025).

93 Y_1 denote the air temperature time series T , Y_2 denote the soil moisture time series SSM , At

94 each grid cell, the information flow from Y_2 to Y_1 is defined as

$$95 T_{2 \rightarrow 1} = \frac{C_{11}C_{12}C_{2,d1} - C_{12}^2C_{1,d1}}{C_{11}^2C_{22} - C_{11}C_{12}^2} \quad (1)$$

96 Where C_{11} and C_{22} are the variances of Y_1 and Y_2 , respectively, and C_{12} is the covariance

97 between them. $C_{1,d1}$ and $C_{2,d1}$ denote the covariances of Y_1 and Y_2 with the differenced term d_1 ,

98 respectively. Here, d_1 is defined as the forward difference of Y_1 :

$$99 d_1 = \frac{Y_{1,i+1} - Y_{1,i}}{\Delta t} \quad (2)$$

100 Where Δt is the time interval, represents the time step. Given the use of monthly data, Δt is



101 set to 1 month, and the corresponding unit of information flow is nats/month.

102 When $T_{2 \rightarrow 1} = 0$, it indicates no identifiable effect of soil moisture on air temperature;
103 conversely, $T_{2 \rightarrow 1} \neq 0$, an effect is present. We focus on its absolute magnitude, $|T_{2 \rightarrow 1}|$, as a
104 measure of causal strength. These grid-by-grid calculations quantify the local influence of soil
105 moisture on air temperature. We used the absolute value of information flow to measure causal
106 strength because our main purpose was to quantify the magnitude of directed influence from soil
107 moisture to temperature. Using the absolute value therefore allowed us to compare the spatial
108 intensity of coupling more clearly across regions.

109 2.2.2 Statistical significance testing

110 To avoid misinterpreting random fluctuations as causal signals, we further assess the statistical
111 significance of the estimated information flow at each grid cell. Under a sufficiently large sample
112 size, the information flow estimator can be approximated as normally distributed around its true
113 value, with variance expressed as:

$$114 \quad \text{Var}(T_{2 \rightarrow 1}) \approx \left(\frac{C_{12}}{C_{11}} \right)^2 \hat{\sigma}_{a_{12}}^2 \quad (3)$$

115 where $\hat{\sigma}_{a_{12}}^2$ is determined from the covariance matrix of the estimated parameter vector $\theta =$
116 $(a_{11}, a_{12}, b_1)^T$, given by

$$117 \quad \text{Cov}(\theta) = (NI)^{-1} \quad (4)$$

118 Here, N is the sample size and I is the Fisher information matrix, whose elements are
119 defined as

$$120 \quad I_{ij} = -\frac{1}{N} \sum_{n=1}^N \frac{\partial^2 \log \rho(Y_{n+1} | Y_n; \hat{\theta})}{\partial \theta_i \partial \theta_j} \quad (5)$$

121 where $\rho(Y_{n+1} | Y_n; \hat{\theta})$ is the conditional probability density function and $\hat{\theta}$ denotes the
122 estimated model parameters. We use $p < 0.05$ as the significance threshold, and only grid cells
123 passing this test are retained for the subsequent spatial analysis and pathway identification.



124 2.2.3 Pathway-consistent identification

125 Identifying the existence of $SSM \rightarrow T$ alone is not sufficient to explain the underlying
126 physical processes. We further decompose this feedback into its intermediate components by
127 separately examining the effects of soil moisture on evapotranspiration and sensible heat flux, as
128 well as the effects of these two fluxes on temperature. Specifically, we consider four causal
129 relationships: $SSM \rightarrow ET$, $SSM \rightarrow SH$, $ET \rightarrow T$, and $SH \rightarrow T$. Based on these sub-processes, we
130 identify two pathway-consistent link types. If both $SSM \rightarrow ET$ and $ET \rightarrow T$ are significant at a
131 given grid cell, we identify an evaporative pathway, denoted as $SSM \rightarrow ET \rightarrow T$. Likewise, if both
132 $SSM \rightarrow SH$ and $SH \rightarrow T$ are significant, we identify a sensible heat pathway, denoted as $SSM \rightarrow$
133 $SH \rightarrow T$. When all four sub-processes are significant, both pathways are considered to operate
134 simultaneously at that location. This decomposition allows us to assess which pathway-consistent
135 structure is more prevalent across regions.

136 2.2.4 Soil-depth and timescale analyses

137 Given that soil moisture feedbacks can vary with depth, season, and background climate
138 conditions, we calculate the information flow separately across four soil layers. This allows us to
139 compare the relative contributions of shallow and deep soil moisture to temperature regulation. To
140 account for seasonal variations, we evaluate the causal strength annually (January–December), as
141 well as specifically for the boreal warm (April–October) and cold (November–March) seasons.
142 These seasonal windows were applied uniformly in the global analysis. Furthermore, to evaluate
143 long-term temporal shifts, we split the 1984–2014 study period into three decadal subperiods (1984–



144 1993, 1994–2003, and 2004–2014). We then compare the spatial patterns and the extent of
145 significantly affected areas across these intervals. Because the sample size in each subperiod is
146 relatively small, this analysis is used mainly to examine the temporal consistency of the spatial
147 patterns.

148 We also examined the persistence of soil moisture effects on temperature. For the lag analysis,
149 we paired soil moisture in month t (SSM_t), with air temperature in month $t + \tau$ ($T_{t+\tau}$), and
150 calculated the corresponding information flow for lag times from 0 to 6 months:

$$151 \quad T_{SSM \rightarrow T}^{(\tau)} = IF(SSM_t, T_{t+\tau}) \quad (6)$$

152 Where $IF(\cdot)$ denotes the information flow operator and τ is the lag time in months. By
153 comparing causal strength across lag times, we identified the persistence and decay characteristics
154 of soil moisture signals in near-surface air temperature. We used $1/e$ of the zero-lag significant
155 fraction as a reference threshold to characterize the persistence of lagged causal signals(Sun et al.,
156 2025).

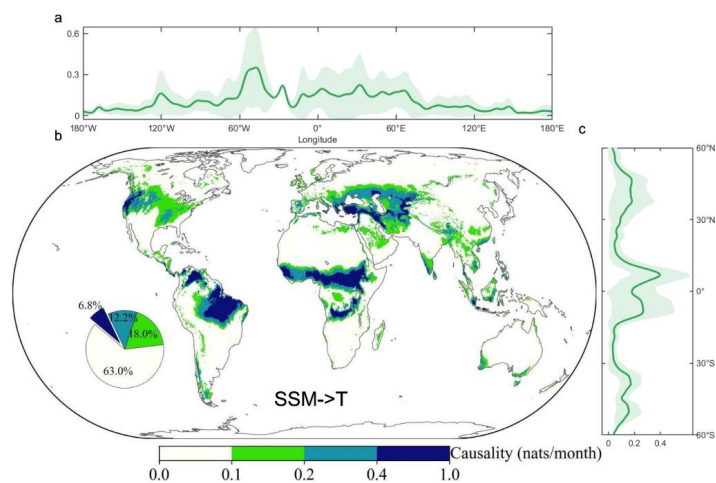
157 3. Results

158 3.1 Global patterns of soil moisture–temperature causality

159 Our results show a statistically significant causal influence of surface soil moisture on near-
160 surface air temperature (Fig. 1). Significant causality (>0.1 , $p < 0.05$) is detected across
161 approximately 37% of the global land area. Most significant areas show intermediate values (0.1–
162 0.4), with 6.8% of the land surface exceeding 0.4 (Fig. 1b). Strong causal signals are primarily
163 concentrated in transitional climate zones, including the African Sahel, the Great Plains of North



164 America, the Indian subcontinent, Central Asia, and parts of Australia (Fig. 1a). Causal strength also
165 exhibits peaks across the northern mid-latitudes and the tropics (Fig. 1a, c). In addition, deeper soil
166 moisture layers continue to exert significant control on temperature in arid and semi-arid regions
167 (Fig. S1), although the total significant area decreases slightly with depth. These results show that
168 significant causal signals are not confined to the shallow surface layer, but remain evident in deeper
169 soil layers, especially in arid and semi-arid regions.



170

171 **Fig. 1 | Significant effects of surface soil moisture on near-surface air temperature.**

172 (a) Longitudinal mean of $SSM \rightarrow T$ causality based on ERA5-Land, with shading indicating ± 1
173 standard deviation.

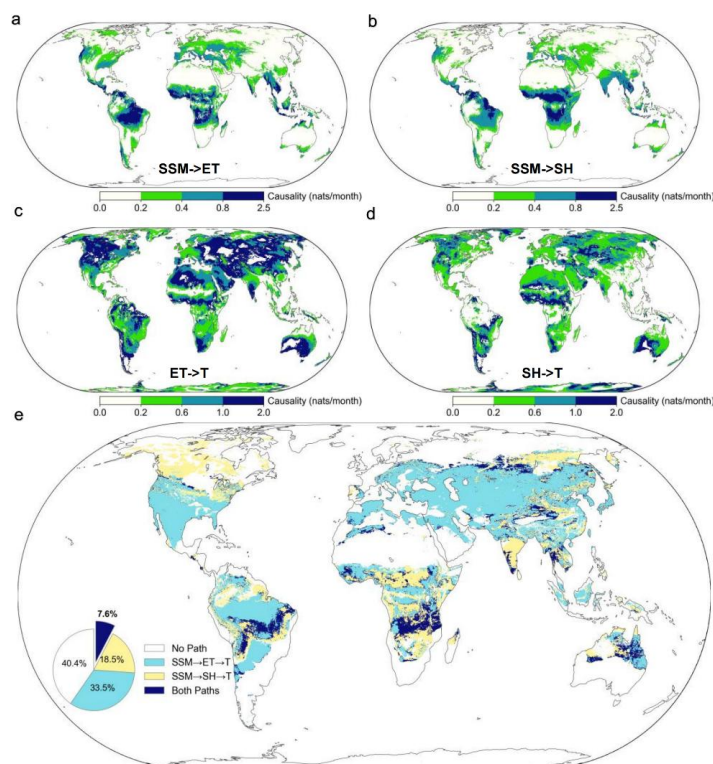
174 (b) Global distribution of effects of surface (0–7 cm) soil moisture on temperature during 1984–
175 2014 (nats/month, $p < 0.05$). The pie chart indicates the proportion of global land area under different
176 strength classes of significant $SSM \rightarrow T$ causality.

177 (c) Same as in (a), but for latitudinal means.



178 3.2 Mechanisms underlying soil moisture–temperature causality

179 The sub-processes linking surface soil moisture to temperature exhibit distinct and statistically
180 significant causal relationships (Fig. 2). Within tropical zones, specifically the Amazon and Congo
181 basins, SSM predominantly regulates evapotranspiration, yielding causal values that exceed 0.8
182 nats/month (Fig. 2a). Conversely, SSM primarily drives sensible heat flux across semi-arid and mid-
183 latitude regions, including the Sahel and parts of Australia (Fig. 2b). This geographic divergence in
184 surface energy partitioning yields differing temperature responses. The influence of
185 evapotranspiration on temperature ($ET \rightarrow T$) is widespread, with the strongest effects occurring in
186 high-latitude regions and tropical rainforests (Fig. 2c). Meanwhile, the influence of sensible heat
187 flux on temperature ($SH \rightarrow T$) is mainly distributed across arid regions and northern Eurasia (Fig.
188 2d). The indirect pathways linking surface soil moisture to temperature differ across climate zones
189 (Fig. 2e). The $SSM \rightarrow ET \rightarrow T$ only pathway is the most widespread, covering 33.5% of the global
190 land surface, primarily in humid tropical and temperate regions. By comparison, the $SSM \rightarrow SH \rightarrow$
191 T only pathway accounts for 18.5% of the land area and is largely concentrated in dry-to-humid
192 transitional zones. Both pathways co-occur over 7.6% of the land surface, notably in southern Africa
193 and parts of South America. Together, these spatial patterns indicate that soil moisture–temperature
194 coupling is more often associated with in humid environments, and through sensible heat exchange
195 in drier regions.



196

197 **Fig. 2 | Causal relationships among the sub-processes linking soil moisture and temperature.**

198 (a) Global distribution of $SSM \rightarrow ET$ effects during 1984–2014 (nats/month, $p < 0.05$).

199 (b–d) Same as in (a), but for the $SSM \rightarrow SH$, $ET \rightarrow T$, and $SH \rightarrow T$ sub-processes, respectively.

200 (e) Global distribution of the causal pathways linking SSM to T. The $SSM \rightarrow ET \rightarrow T$ (or $SSM \rightarrow$

201 $SH \rightarrow T$) pathway is identified in regions where both adjacent sub-processes are significant. Areas

202 where all four causal links are significant are designated as dual-pathway regions. The inset pie

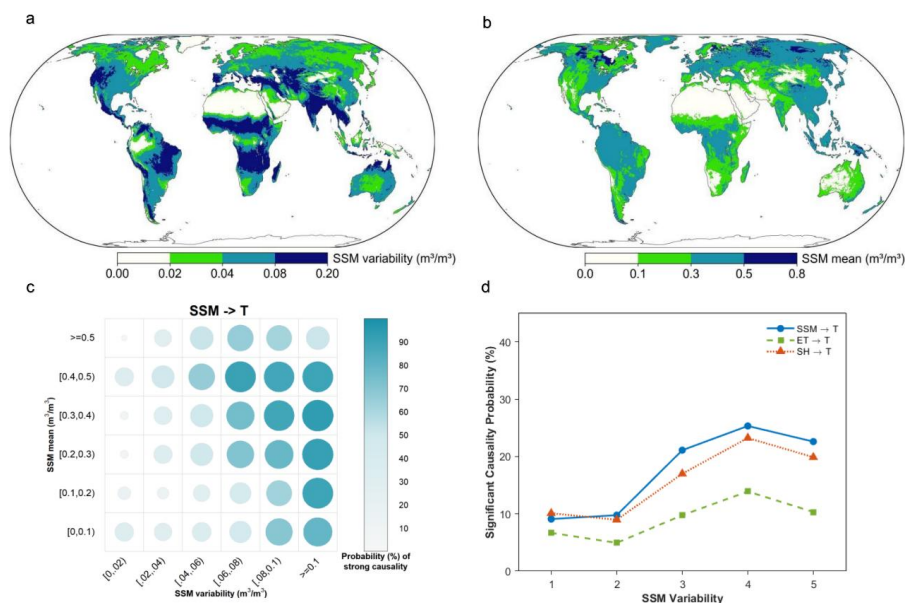
203 chart shows the proportion of global land area associated with each pathway type.

204



205 3.3 Dependence of causal strength on soil moisture variability

206 We further investigate how the spatial characteristics of SSM influence the strength of land–
207 atmosphere causal coupling (Fig. 3). Strong causal feedbacks closely follow the spatial pattern of
208 SSM variability (Fig. 3a), whereas no clear correspondence is found with the climatological mean
209 state of SSM (Fig. 3b). As SSM variability increases, the probability of significant causal feedback
210 rises sharply in a nonlinear manner (Fig. 3c). Within regions of high variability ($\geq 0.08 \text{ m}^3/\text{m}^3$),
211 this probability increases from less than 10% to more than 90%. These results suggest that soil
212 moisture variability is more strongly associated with the probability of significant SSM–T coupling
213 than the mean state. Increased variability triggers non-stationary surface energy perturbations,
214 thereby generating a prominent causal signal that persists against complex climate backgrounds.
215 The occurrence probabilities of all three causal pathways increase with rising soil moisture
216 variability (Fig. 3d, Fig. S6–S7). Together, these findings identify soil moisture variability as a major
217 controlling factor in the emergence and strength of causal land–atmosphere feedbacks.



218

219 **Fig. 3 | Soil moisture variability as a primary determinant of causal coupling probability.**

220 (a) Spatial distribution of surface SSM variability (m^3/m^3) during 1984–2014, defined as the
 221 standard deviation of monthly mean SSM.

222 (b) Spatial distribution of mean surface SSM (m^3/m^3) during 1984–2014.

223 (c) Probability of significant $SSM \rightarrow T$ causality across two-dimensional bins of SSM variability
 224 and mean state. Probability is defined as the fraction of significant grid cells relative to the total
 225 number of grid cells within each bin.

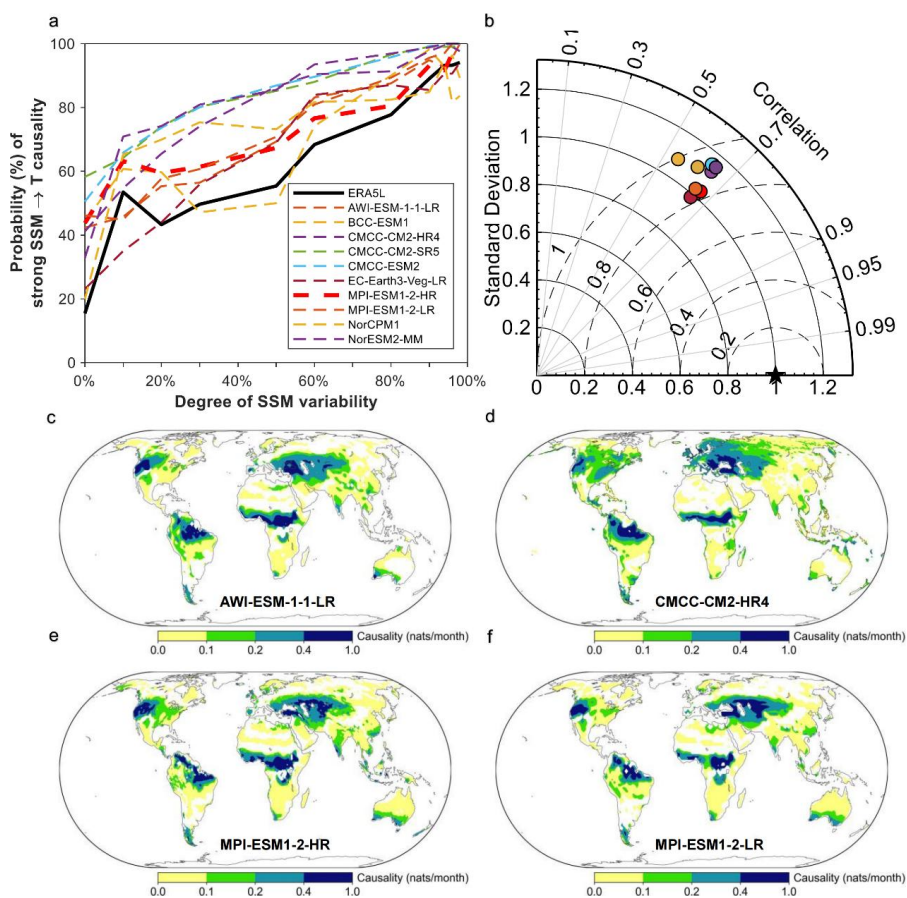
226 (d) Probability of significant $SSM \rightarrow T$, $ET \rightarrow T$, and $SH \rightarrow T$ causality across different SSM
 227 variability intervals. Levels 1–5 represent increasing soil moisture variability percentile bins (0–
 228 33.3%, 33.3–50%, 50–66.7%, 66.7–83.3%, and 83.3–100%).

229



230 3.4 CMIP6 model evaluation

231 We assessed the capacity of 10 CMIP6 models to reproduce causal links between surface soil
232 moisture and temperature. Although the models capture the qualitative increase in feedback strength
233 under high soil moisture variability, they suffer from a systematic bias: overestimating the likelihood
234 of significant causality (Fig. 4a). All evaluated models produce anomalously high coupling
235 probabilities across all variability ranges when compared to reanalysis data (Fig. 4a). Taylor diagram
236 analysis further confirms this, showing a consistent departure from observational benchmarks (Fig.
237 4b). Furthermore, while representative models identify key spatial hotspots, they simulate an
238 exaggerated extent of influence (Fig. 4c–f, Fig. S8–S9). In summary, CMIP6 models reproduce the
239 overall spatial pattern of soil moisture–temperature coupling, but they tend to overestimate its
240 strength and spatial extent.



241

242 **Fig. 4 | CMIP6 model evaluation for SSM–temperature causal coupling.**

243 (a) Causal probability versus SSM variability in ERA5-Land and CMIP6 models.

244 (b) Taylor diagram of model performance relative to ERA5-Land (black star).

245 (c–f) Global distributions of significant causal influence for four representative models. Causal

246 effects are measured by information flow; only statistically significant regions are displayed.



247 4. Discussion

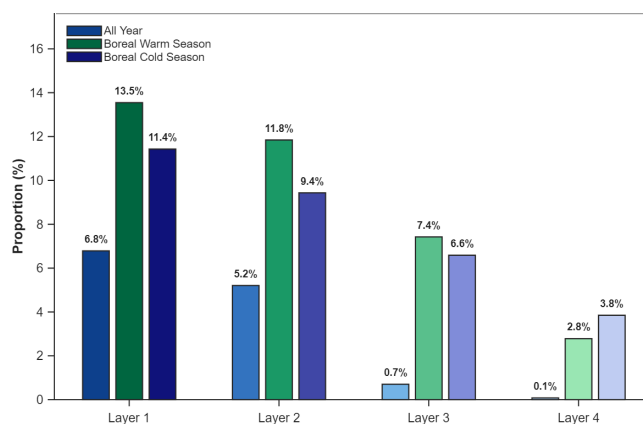
248 4.1 Widespread causal coupling across seasons and soil depths

249 From a causal perspective, our results identify a widespread influence of surface soil moisture
250 on air temperature, particularly across dry–wet transition zones (Day et al., 2025; Hsu and Dirmeyer,
251 2023; Miralles et al., 2012). Crucially, we show that soil moisture is not simply a passive correlate
252 of temperature anomalies but an active driver of near-surface thermal states. This causal architecture
253 remains robust across various sensitivity tests, confirming that the identified SSM–T relationship is
254 not an artifact of specific datasets, soil depths, or temporal windows. Independent validation using
255 the GLEAM satellite-based product shows spatial congruence with ERA5-Land (Fig. S10). This
256 causal structure is also temporally stable across decades. The main spatial features of SSM–T
257 causality remain highly consistent over the three subperiods analysed (Fig. S4). These findings
258 suggest that this feedback is not solely controlled by short-term climate anomalies in a particular
259 period, but may represent a relatively stable feature of global land–atmosphere coupling. From a
260 vertical perspective, the feedback is most extensive in the surface layer, but deeper soil moisture
261 continues to exert significant influence over large regions, particularly in arid and semi-arid
262 environments (Fig. S1). This suggests that the influence of soil moisture on temperature is not
263 confined to a thin surface layer, but instead reflects a coupled process involving both shallow and
264 deep soil water. Deep soil moisture may prolong this regulation by sustaining root-zone water supply
265 and vegetation transpiration (Rahmati et al., 2024; Seneviratne et al., 2006).

266



267 Seasonality exerts a strong control on this causal feedback (Day et al., 2025; Dirmeyer et al.,
268 2018; Jaeger and Seneviratne, 2011) (Fig. S2-S3). Across all soil depths, causal strength is much
269 higher during the boreal warm season than the annual mean, while it stays weak in the cold season
270 (Fig. 5, Fig. S2-S3). This difference suggests that the role of soil moisture depends not only on
271 water availability, but also on the background state of surface energy exchange. The boreal warm
272 season is generally marked by higher net radiation, greater evaporative demand, and more active
273 vegetation. Under these conditions, soil moisture anomalies are more easily transferred to the
274 atmosphere through evapotranspiration and sensible heat partitioning. In contrast, during the cold
275 season, low energy availability and reduced vegetation activity weaken the link between soil
276 moisture and air temperature. Thus, the SSM-T causal relationship is a seasonal hydrothermal
277 coupling process that peaks during the boreal warm season.



278

279 **Fig. 5 | Fraction of significant causal relationships across soil layers and seasons.**

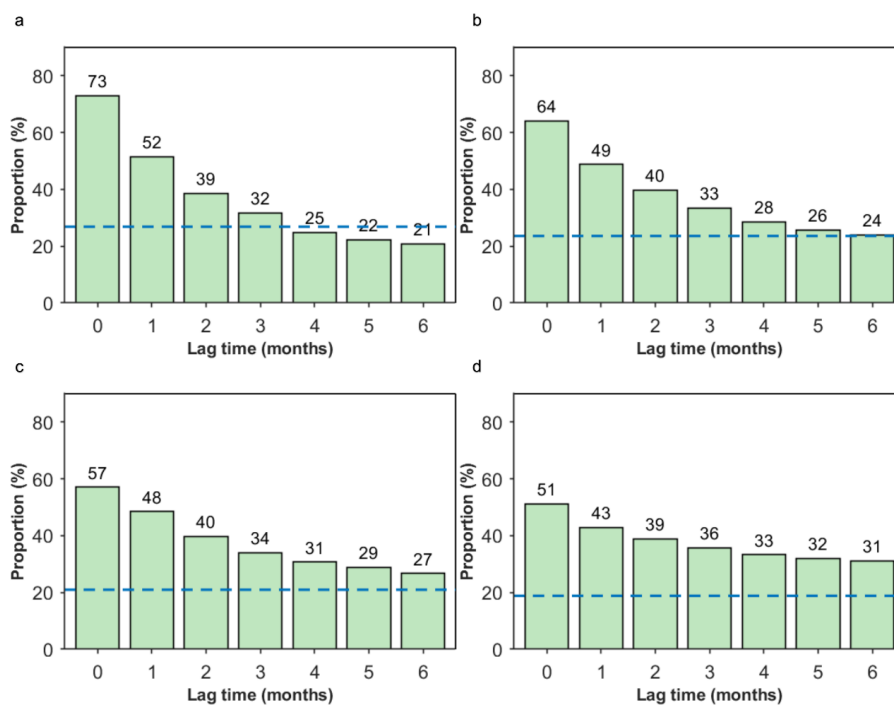
280 The percentage of land area exhibiting significant causality for Layers 1–4 is compared across the

281 full year (Jan–Dec), boreal warm season (Apr–Oct), and boreal cold season (Nov–Mar).

282



283 Lag analysis further suggests that this feedback is not instantaneous(Lorenz et al., 2010;
284 Rahmati et al., 2024; Seneviratne et al., 2006). Significant causal signals from surface soil moisture
285 persist for 1–2 months (Fig. 6a), and this persistence extends even longer in deeper layers (Fig. 6d).
286 This indicates that soil moisture regulates temperature not only concurrently, but also over
287 subsequent months through soil water memory(McColl et al., 2017; Rahmati et al., 2024). Deep soil
288 moisture may act as an important memory reservoir. Even when surface moisture fluctuates rapidly
289 over short timescales, water stored in deeper layers may continue to affect near-surface temperature,
290 which is consistent with the role of sustained root-zone water supply and vegetation transpiration.
291 This suggests that soil moisture anomalies may influence near-surface temperature over multiple
292 months. Given its consistency across various spatial and temporal scales, these results suggest that
293 soil moisture is not merely a passive response to temperature variability, but may also play an active
294 role in shaping near-surface thermal conditions.



295

296 **Fig. 6 | Persistence of SSM-T causality across soil layers and lag times.**

297 (a-d) Percentage of grid cells showing significant $SSM \rightarrow T$ causality for Layers 1-4 at lag times
 298 of 0 to 6 months. The horizontal dashed line indicates $1/e$ of the zero-lag significant fraction for
 299 each layer and is used here as a reference threshold for persistence.

300 Our results further show that soil moisture affects temperature primarily through latent and
 301 sensible heat fluxes, with the dominant pathway varying by region. In humid tropical and temperate
 302 regions, the $SSM \rightarrow ET \rightarrow T$ pathway is stronger, indicating that soil moisture is more often
 303 associated with evapotranspiration (Dirmeyer, 2011; Fu et al., 2024; Guillod et al., 2014; Hsu and
 304 Dirmeyer, 2023). Conversely, in semi-arid and transitional climates, the $SSM \rightarrow SH \rightarrow T$ pathway
 305 is more pronounced, suggesting that soil moisture anomalies are more readily translated into
 306 temperature changes through sensible heat transfer. This indicates that SSM-T coupling is not



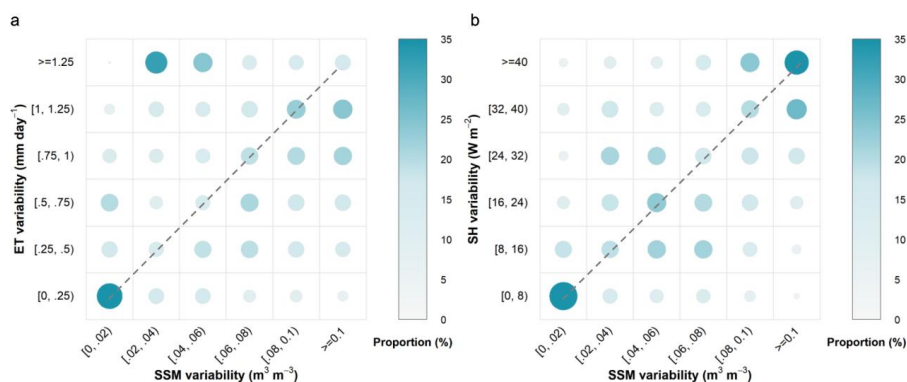
307 governed by a single mechanism, but is a multi-pathway process shaped by regional hydroclimate.
308 Therefore, future analyses of compound droughts and heatwaves must account for the dominant
309 energy-flux pathway in each region.

310 4.2 Soil moisture variability drives causal emergence

311 Our results show that the key factor controlling the strength of soil moisture–temperature
312 causal feedback is not the mean state of SSM, but its variability(Holmes et al., 2017; Hsu and
313 Dirmeyer, 2023; Nouri and Homae, 2021; Sun et al., 2025). This finding is robust across different
314 soil depths (Fig. S5) and is further validated by the GLEAM dataset (Fig. S11). Increasing SSM
315 variability substantially raises the probability of causal emergence. Statistically, as SSM variability
316 increases, the probability of significant causality rises rapidly. High variability in SSM easily drives
317 changes in ET and SH (Fig. S6). These changes in ET and SH then significantly affect temperature
318 (Fig. S7). These results suggest that soil moisture variability helps control temperature by affecting
319 how energy is shared at the land surface. This finding further indicates that while the mean state of
320 soil moisture primarily reflects the long-term hydroclimatic background, it does not necessarily
321 trigger strong land–atmosphere feedbacks. By contrast, greater soil moisture variability implies
322 more pronounced fluctuations in surface water availability. These fluctuations are more likely to
323 perturb latent and sensible heat fluxes(Dirmeyer, 2011; Fu et al., 2024; Humphrey et al., 2021),
324 thereby generating stronger temperature responses (Fig. 7). This relationship also helps explain why
325 many moderately wet regions emerge as hotspots of land–atmosphere coupling. Therefore, future
326 assessments of land–atmosphere feedbacks and heat risks should account not only for shifts in mean
327 soil moisture but also for changes in its variability(Gu et al., 2025; Maraun et al., 2025; Zhou et al.,



328 2024).



329

330 **Fig. 7 | Relationship between $SSM \rightarrow T$ causality and the variability of SSM and intermediate**

331 **variables (ET/SH).**

332 (a) Probability of significant $SSM \rightarrow T$ causality across two-dimensional bins of SSM variability

333 and ET variability. Probability is defined as the fraction of significant grid cells relative to the total

334 number of grid cells within each bin.

335 (b) Same as in (a), but for two-dimensional bins of SSM variability and SH variability.

336 4.3 Model overestimation of coupling strength

337 Comparison of the 10 CMIP6 models with ERA5-Land shows a common bias in simulated

338 land-atmosphere coupling (Fig. 4). The models generally reproduce the tendency for stronger causal

339 feedbacks under larger SSM variability. However, they systematically overestimate the coupling

340 strength. For a given level of SSM variability, all models simulate a higher probability of significant

341 causality than ERA5-Land. The models also capture the main hotspot, but they consistently

342 overestimate the spatial extent of significant influence (Fig. S8–S9). This suggests that the models

343 represent the basic physical relationship, but exaggerate both the strength and extent of the coupling.



344 This bias is likely to have multiple causes. One possibility is that stomatal conductance or resistance
345 in the models is too sensitive to soil water stress(Fu et al., 2024; Giardina et al., 2025; Green et al.,
346 2024). Another is that boundary-layer processes respond too strongly to surface heating. Both effects
347 would enhance land–atmosphere feedbacks. As a result, the models may amplify the warming effect
348 of soil drought too strongly during heat extremes. This bias has important implications for climate
349 risk assessment. If models overestimate the causal influence of soil moisture on temperature, they
350 may also overstate the extent to which drought intensifies future hot extremes and heatwaves(Berg
351 et al., 2016; Maraun et al., 2025; Papagiannopoulou et al., 2017; Ukkola et al., 2020; Wouters et al.,
352 2022; Zhou et al., 2024). Such uncertainty should be considered carefully when using climate
353 models to assess future changes in land–atmosphere coupling and their impacts on extreme heat.

354 4.4 Limitations and outlook

355 Although this study reveals the influence of global soil moisture on near-surface air
356 temperature from a causal perspective, several limitations should be noted. First, the reanalysis
357 datasets used here still contain uncertainties in observation-sparse regions, which may affect local
358 estimates of causal strength. Second, our analysis is based on monthly data. This timescale is well
359 suited to identifying persistent intraseasonal to intermonthly feedbacks and associated soil moisture
360 memory, but is less able to capture the rapid land–atmosphere coupling responses linked to extreme
361 heat, flash droughts and heatwaves at shorter timescales. Future work should therefore incorporate
362 daily data to examine how causal strength depends on timescale(Phillips and Klein, 2014;
363 Santanello et al., 2018). Third, we focus on evapotranspiration and sensible heat as the two main
364 pathways linking soil moisture to temperature. Also, the causal relationships identified here should



365 be interpreted as statistically directed influences under the Liang–Kleeman information flow
366 framework, rather than fully isolated physical causation. This framework is useful for interpreting
367 regional differences, but it simplifies a more complex system. In reality, land–atmosphere coupling
368 is also influenced by radiation, vegetation physiology and human activities. The current pathway
369 decomposition therefore cannot fully resolve all intermediary processes. Future work could include
370 additional variables to construct a more complete multivariate causal network and better identify
371 the dominant controls on land–atmosphere feedbacks across climate regimes(Hagan et al., 2019;
372 Liang, 2016; Sun et al., 2025).

373 5. Conclusions

374 Using the Liang–Kleeman information flow framework, we show that soil moisture has a
375 widespread directed influence on near-surface air temperature across global land. This coupling is
376 more strongly associated with soil moisture variability than with mean state, is more often linked to
377 evaporative processes than to sensible-heat-related processes, and shows more persistent lagged
378 effects in deeper soil layers. These results should be interpreted as large-scale evidence for
379 statistically directed land–atmosphere coupling rather than fully isolated physical causation, but
380 they provide useful insight for climate model evaluation and for improving the understanding of
381 soil-moisture effects on heat extremes.

382 Data availability

383 ERA5-Land data are available from the Copernicus Climate Data Store



384 (<https://cds.climate.copernicus.eu/datasets/reanalysis-era5-land-monthly-means?tab=download>).

385 GLEAM v4.2a data are available from the Global Land Evaporation Amsterdam Model data portal

386 (<https://www.gleam.eu/>). CMIP6 historical simulations are available from the Copernicus Climate

387 Data Store (<https://cds.climate.copernicus.eu/datasets/projections-cmip6?tab=download>). The

388 processed data used to support the findings of this study are available from the corresponding author

389 upon reasonable request.

390 Code availability

391 The code used for data preprocessing, Liang–Kleeman information flow calculation, pathway

392 identification, CMIP6 model evaluation, and figure generation is available from the corresponding

393 author upon reasonable request.

394 Author contributions

395 XG and JH conceived the study. XG performed the data processing, analysis, visualization, and

396 manuscript drafting. JH supervised the study, contributed to the methodology, and revised the

397 manuscript. HS, XZ, XS, LL, ZC, and GL contributed to data interpretation, discussion, and

398 manuscript revision. All authors reviewed and approved the final manuscript.

399 Competing interests

400 The authors declare that they have no conflict of interest.



401 **Financial support**

402 This study was funded by the Sichuan Science and Technology Department (No. 2026NSFSC1107).

403 **Reference**

- 404 Berg, A., Findell, K., Lintner, B., Giannini, A., Seneviratne, S.I., van den Hurk, B., Lorenz, R.,
405 Pitman, A., Hagemann, S., Meier, A., Cheruy, F., Ducharne, A., Malyshev, S., Milly, P.C.D.,
406 2016. Land–atmosphere feedbacks amplify aridity increase over land under global warming.
407 *Nat. Clim. Change* 6, 869–874. <https://doi.org/10.1038/nclimate3029>
- 408 Chiang, F., Mazdiyasi, O., AghaKouchak, A., 2021. Evidence of anthropogenic impacts on global
409 drought frequency, duration, and intensity. *Nat. Commun.* 12, 2754.
410 <https://doi.org/10.1038/s41467-021-22314-w>
- 411 Day, J.J., Vitart, F., Stockdale, T., de Rosnay, P., Ardilouze, C., Peano, D., Sanna, A., Fröhlich, K.,
412 Andrews, M., 2025. Soil-moisture-atmosphere coupling hotspots and their representation
413 in seasonal forecasts of boreal summer. *Clim. Dyn.* 63, 275.
414 <https://doi.org/10.1007/s00382-025-07753-1>
- 415 Dirmeyer, P.A., 2011. The terrestrial segment of soil moisture-climate coupling: SOIL MOISTURE-
416 CLIMATE COUPLING. *Geophysical Research Letters* 38, n/a-n/a.
417 <https://doi.org/10.1029/2011GL048268>
- 418 Dirmeyer, P.A., Halder, S., Bombardi, R., 2018. On the harvest of predictability from land states in
419 a global forecast model. *Journal of Geophysical Research: Atmospheres* 123.
420 <https://doi.org/10.1029/2018JD029103>
- 421 Ebert-Uphoff, I., Deng, Y., 2012. Causal discovery for climate research using graphical models.
422 *Journal of Climate* 25, 5648–5665. <https://doi.org/10.1175/JCLI-D-11-00387.1>
- 423 Fu, Z., Ciais, P., Wigneron, J.-P., Gentile, P., Feldman, A.F., Makowski, D., Viovy, N., Kemanian,
424 A.R., Goll, D.S., Stoy, P.C., Prentice, I.C., Yakir, D., Liu, L., Ma, H., Li, Xiaojun, Huang,
425 Y., Yu, K., Zhu, P., Li, Xing, Zhu, Z., Lian, J., Smith, W.K., 2024. Global critical soil
426 moisture thresholds of plant water stress. *Nat. Commun.* 15, 4826.
427 <https://doi.org/10.1038/s41467-024-49244-7>
- 428 Gevaert, A.I., Miralles, D.G., Jeu, R.A.M. de, Schellekens, J., Dolman, A.J., 2018. Soil moisture-
429 temperature coupling in a set of land surface models. *Journal of Geophysical Research:*
430 *Atmospheres* 123, 1481–1498. <https://doi.org/10.1002/2017JD027346>
- 431 Giardina, F., Padrón, R.S., Stocker, B.D., Schumacher, D.L., Seneviratne, S.I., 2025. Large biases
432 in the frequency of water limitation across earth system models. *Commun. Earth Environ.*
433 6, 469. <https://doi.org/10.1038/s43247-025-02426-7>
- 434 Green, J.K., Zhang, Y., Luo, X., Keenan, T.F., 2024. Systematic underestimation of canopy
435 conductance sensitivity to drought by Earth system models. *AGU Advances* 5,
436 e2023AV001026. <https://doi.org/10.1029/2023AV001026>



- 437 Gu, L., Schumacher, D.L., Fischer, E.M., Slater, L.J., Yin, J., Sippel, S., Chen, J., Liu, P., Knutti, R.,
438 2025. Flash drought impacts on global ecosystems amplified by extreme heat. *Nat. Geosci.*
439 18, 709–715. <https://doi.org/10.1038/s41561-025-01719-y>
- 440 Guillod, B.P., Orłowsky, B., Miralles, D., Teuling, A.J., Blanken, P.D., Buchmann, N., Ciais, P., Ek,
441 M., Findell, K.L., Gentine, P., Lintner, B.R., Scott, R.L., Van den Hurk, B., I. Seneviratne,
442 S., 2014. Land-surface controls on afternoon precipitation diagnosed from observational
443 data: uncertainties and confounding factors. *Atmos. Chem. Phys.* 14, 8343–8367.
444 <https://doi.org/10.5194/acp-14-8343-2014>
- 445 Hagan, D.F.T., Wang, G., Liang, X.S., Dolman, H.A.J., 2019. A time-varying causality formalism
446 based on the liang–kleeman information flow for analyzing directed interactions in
447 nonstationary climate systems. *Journal of Climate* 32, 7521–7537.
448 <https://doi.org/10.1175/JCLI-D-18-0881.1>
- 449 Hirschi, M., Seneviratne, S.I., Alexandrov, V., Boberg, F., Boroneant, C., Christensen, O.B.,
450 Formayer, H., Orłowsky, B., Stepánek, P., 2011. Observational evidence for soil-moisture
451 impact on hot extremes in southeastern Europe. *Nat. Geosci.* 4, 17–21.
452 <https://doi.org/10.1038/ngeo1032>
- 453 Holmes, A., Rüdiger, C., Mueller, B., Hirschi, M., Tapper, N., 2017. Variability of soil moisture
454 proxies and hot days across the climate regimes of Australia. *Geophysical Research Letters*
455 44, 7265–7275. <https://doi.org/10.1002/2017GL073793>
- 456 Hsu, H., Dirmeyer, P.A., 2023. Soil moisture–evaporation coupling shifts into new gears under
457 increasing CO₂. *Nat. Commun.* 14, 1162. <https://doi.org/10.1038/s41467-023-36794-5>
- 458 Humphrey, V., Berg, A., Ciais, P., Gentine, P., Jung, M., Reichstein, M., Seneviratne, S.I.,
459 Frankenberg, C., 2021. Soil moisture–atmosphere feedback dominates land carbon uptake
460 variability. *Nature* 592, 65–69. <https://doi.org/10.1038/s41586-021-03325-5>
- 461 Jaeger, E.B., Seneviratne, S.I., 2011. Impact of soil moisture–atmosphere coupling on European
462 climate extremes and trends in a regional climate model. *Clim. Dyn.* 36, 1919–1939.
463 <https://doi.org/10.1007/s00382-010-0780-8>
- 464 Liang, X.S., 2016. Information flow and causality as rigorous notions *ab initio*. *Phys. Rev. E* 94,
465 052201. <https://doi.org/10.1103/PhysRevE.94.052201>
- 466 Lorenz, R., Jaeger, E.B., Seneviratne, S.I., 2010. Persistence of heat waves and its link to soil
467 moisture memory. *Geophysical Research Letters* 37, 2010GL042764.
468 <https://doi.org/10.1029/2010GL042764>
- 469 Maraun, D., Schiemann, R., Ossó, A., Jury, M., 2025. Changes in event soil moisture–temperature
470 coupling can intensify very extreme heat beyond expectations. *Nat. Commun.* 16, 734.
471 <https://doi.org/10.1038/s41467-025-56109-0>
- 472 McColl, K.A., Alemohammad, S.H., Akbar, R., Konings, A.G., Yueh, S., Entekhabi, D., 2017. The
473 global distribution and dynamics of surface soil moisture. *Nat. Geosci.* 10, 100–104.
474 <https://doi.org/10.1038/ngeo2868>
- 475 Miralles, D.G., Bonte, O., Koppa, A., Baez-Villanueva, O.M., Tronquo, E., Zhong, F., Beck, H.E.,
476 Hulsman, P., Dorigo, W., Verhoest, N.E.C., Haghdoust, S., 2025. GLEAM4: global land
477 evaporation and soil moisture dataset at 0.1° resolution from 1980 to near present. *Sci Data*
478 12, 416. <https://doi.org/10.1038/s41597-025-04610-y>
- 479 Miralles, D.G., Gentine, P., Seneviratne, S.I., Teuling, A.J., 2019. Land–atmospheric feedbacks



- 480 during droughts and heatwaves: state of the science and current challenges. *Ann. N. Y. Acad.*
481 *Sci.* 1436, 19–35. <https://doi.org/10.1111/nyas.13912>
- 482 Miralles, D.G., van den Berg, M.J., Teuling, A.J., de Jeu, R. a. M., 2012. Soil moisture-temperature
483 coupling: a multiscale observational analysis. *Geophys. Res. Lett.* 39, 2012GL053703.
484 <https://doi.org/10.1029/2012GL053703>
- 485 Nouri, M., Homae, M., 2021. Contribution of soil moisture variations to high temperatures over
486 different climatic regimes. *Soil Tillage Res.* 213, 105115.
487 <https://doi.org/10.1016/j.still.2021.105115>
- 488 Papagiannopoulou, C., Miralles, D.G., Dorigo, W.A., Verhoest, N.E.C., Depoorter, M., Waegeman,
489 W., 2017. Vegetation anomalies caused by antecedent precipitation in most of the world.
490 *Environ. Res. Lett.* 12, 074016. <https://doi.org/10.1088/1748-9326/aa7145>
- 491 Phillips, T.J., Klein, S.A., 2014. Land-atmosphere coupling manifested in warm-season
492 observations on the U.S. southern great plains. *Journal of Geophysical Research:*
493 *Atmospheres* 119, 509–528. <https://doi.org/10.1002/2013JD020492>
- 494 Rahmati, M., Amelung, W., Brogi, C., Dari, J., Flammini, A., Bogena, H., Brocca, L., Chen, H.,
495 Groh, J., Koster, R.D., McColl, K.A., Montzka, C., Moradi, S., Rahi, A., S, F.S., Vereecken,
496 H., 2024. Soil Moisture Memory: State-Of-The-Art and the Way Forward. *Reviews of*
497 *Geophysics* 62, e2023RG000828. <https://doi.org/10.1029/2023RG000828>
- 498 Runge, J., Bathiany, S., Bolt, E., Camps-Valls, G., Coumou, D., Deyle, E., Glymour, C., Kretschmer,
499 M., Mahecha, M.D., Muñoz-Mari, J., van Nes, E.H., Peters, J., Quax, R., Reichstein, M.,
500 Scheffer, M., Schölkopf, B., Spirtes, P., Sugihara, G., Sun, J., Zhang, K., Zscheischler, J.,
501 2019. Inferring causation from time series in Earth system sciences. *Nat Commun* 10, 2553.
502 <https://doi.org/10.1038/s41467-019-10105-3>
- 503 Santanello, J.A., Dirmeyer, P.A., Ferguson, C.R., Findell, K.L., Tawfik, A.B., Berg, A., Ek, M.,
504 Gentine, P., Guillod, B.P., Heerwaarden, C. van, Roundy, J., Wulfmeyer, V., 2018. Land–
505 atmosphere interactions: the LoCo perspective. *Bulletin of the American Meteorological*
506 *Society* 99, 1253–1272. <https://doi.org/10.1175/BAMS-D-17-0001.1>
- 507 Schwingshackl, C., Hirschi, M., Seneviratne, S.I., 2017. Quantifying Spatiotemporal Variations of
508 Soil Moisture Control on Surface Energy Balance and Near-Surface Air Temperature.
509 *Journal of Climate* 30, 7105–7124. <https://doi.org/10.1175/JCLI-D-16-0727.1>
- 510 Seneviratne, S.I., Corti, T., Davin, E.L., Hirschi, M., Jaeger, E.B., Lehner, I., Orlowsky, B., Teuling,
511 A.J., 2010. Investigating soil moisture–climate interactions in a changing climate: A review.
512 *Earth Sci. Rev.* 99, 125–161. <https://doi.org/10.1016/j.earscirev.2010.02.004>
- 513 Seneviratne, S.I., Koster, R.D., Guo, Z., Dirmeyer, P.A., Kowalczyk, E., Lawrence, D., Liu, P.,
514 Mocko, D., Lu, C.-H., Oleson, K.W., Verseghy, D., 2006. Soil moisture memory in AGCM
515 simulations: analysis of global land–atmosphere coupling experiment (GLACE) data.
516 *Journal of Hydrometeorology* 7, 1090–1112. <https://doi.org/10.1175/JHM533.1>
- 517 Sugihara, G., May, R., Ye, H., Hsieh, C., Deyle, E., Fogarty, M., Munch, S., 2012. Detecting
518 Causality in Complex Ecosystems. *Science* 338, 496–500.
519 <https://doi.org/10.1126/science.1227079>
- 520 Sun, P., Liu, R., Yao, R., Gu, X., Gulakhmadov, A., Kong, D., Zhang, X., 2025. Propagation
521 threshold from meteorological to agricultural drought and its potential influence factors.
522 *Journal of Hydrology* 655, 132920. <https://doi.org/10.1016/j.jhydrol.2025.132920>



- 523 Ukkola, A.M., De Kauwe, M.G., Roderick, M.L., Abramowitz, G., Pitman, A.J., 2020. Robust future
524 changes in meteorological drought in CMIP6 projections despite uncertainty in
525 precipitation. *Geophys. Res. Lett.* 47, e2020GL087820.
526 <https://doi.org/10.1029/2020GL087820>
- 527 Wouters, H., Keune, J., Petrova, I.Y., Van Heerwaarden, C.C., Teuling, A.J., Pal, J.S., Vilà-Guerau
528 De Arellano, J., Miralles, D.G., 2022. Soil drought can mitigate deadly heat stress thanks
529 to a reduction of air humidity. *Sci. Adv.* 8, eabe6653.
530 <https://doi.org/10.1126/sciadv.abe6653>
- 531 Zhou, J., Milošević, D., Teuling, A.J., 2025. Future exposure to moist heat extremes linked to soil
532 dryness. *npj Clim. Atmos. Sci.* 8, 374. <https://doi.org/10.1038/s41612-025-01252-0>
- 533 Zhou, J., Teuling, A.J., Seneviratne, S.I., Hirsch, A.L., 2024. Soil moisture-temperature coupling
534 increases population exposure to future heatwaves. *Earth's Future* 12, e2024EF004697.
535 <https://doi.org/10.1029/2024EF004697>

536